Two-dimensional FEM Analysis of Brillouin Gain Spectra in Acoustic Guiding and Antiguiding Single Mode Optical Fibers

Y. Sikali Mamdem[1*], X. Pheron[2], F.Taillade[3], Y. Jaouën[4], R. Gabet[4], V. Lanticq[1(+)], G. Moreau[1], A. Boukenter[5], Y. Ouerdane[5], S. Lesoille[2], J. Bertrand[2]
[1]EDF R&D, [2]ANDRA, [3]LCPC, [4] Institut Telecom/Telecom ParisTech, [5]Laboratoire Hubert Curien
[(+)] Now with CEMENTYS
*Corresponding author: EDF R&D, 6 quai Watier 78401 Chatou, France,
Email: yolande.sikali-mamdem@telecom-paristech.fr

Abstract: The analysis of optical and acoustic properties of optical fibers is required for accurate Brillouin gain spectrum (BGS) determination. We present a full modal-analysis of the guided optical and acoustic modes based on a two-dimensional finite-element method (2D-FEM) for BGS calculation using COMSOL Multiphysics. We believe that this method will be helpful in analyzing and designing special fibers for applications, such as fiber amplifiers with significant SBS (Stimulated Brillouin Scattering) suppression or Brillouin-based fiber sensors. The model is adapted for BGS evaluation of any single mode fiber (in term of optical mode) based on its profile, namely its geometry, and its doping composition. Compared to standard multi-layer methods limited to axially-symmetric fibers [1], the 2D-FEM analysis enables the BGS computation even for more complicated geometries, such as PANDA polarization-maintaining fiber where the optical index and the material stress are azimuthally dependant. The results of numerical modeling have shown good agreement with measured Brillouin spectra for different types of silica fibers. Examples are given for a standard GeO_2-doped core fiber (standard fiber for telecommunication applications), Fluor-doped cladding fiber (acoustic anti-waveguide) and PANDA fiber.

Keywords: Optical fibers, Stimulated Brillouin Scattering, acoustic waveguide, finite-element analysis.

1. Introduction

Brillouin Scattering in optical fibers is a nonlinear process caused by interaction between optical wave and acoustic waves. It manifests through the generation of a backward-propagating Stokes wave which the frequency is downshifted by ~11GHz for a 1.55µm optical signal. The Brillouin scattering effect is a limitation for optical systems as fiber lasers [2] or transmission systems [3, 4] when sources are highly coherent. However, it can also be used in optical sensors for strain and temperature measurements [5] or optical signal processing systems [6].

The Brillouin gain spectrum (BGS) properties are strongly related to interaction between the optical mode and the different acoustic modes guided in the core (acoustic waveguides) or guided in the cladding (acoustic anti-waveguides) [7]. As the Brillouin scattering properties are highly dependent of the doping composition profile, a precise computing tool to predict BGS is required.

Multi-layers methods are perfectly adapted for the BGS calculation of axially-symmetric fibers [1, 7]. It's well-known that software based on a finite-element method, such as COMSOL Multiphysics solve 2D electromagnetic problems. Thus it is an excellent tool to extend BGS computation for any azimutal doping- and stress-dependant fibers such as polarization maintaining fibers [8, 9]. We present as an example the obtained BGS of a standard single fiber (GeO_2 core doping). The very good agreement with corresponding BGS measurements allows validation of the developed 2D-FEM computation model. The acoustic waves in a Fluor-doped cladding fiber act as anti-waveguides. Despite this difficulty, the BGS of a pure Fluor-doped cladding fiber based on its measured refractive index profile has been calculated and compared to BGS measurements. Finally, the calculated BGS of a polarization-maintaining fiber (PANDA type) is presented.

2. Theoretical background

A BGS calculation requires a rigorous determination of the acoustic-optical interaction, i.e. overlap between optical and acoustic modes.

In single-mode fiber only the fundamental optical LP_{01} mode is propagated. It results that the only excited acoustic modes are then the longitudinal acoustic modes L_{0m} with no azimuthal dependence. The properties of the optical and longitudinal acoustic modes have been obtained by solving the 2D scalar-wave equations of the optical propagation (1) and the mechanical equations (2) [7, 9]:

$$\Delta_t^2 E + \left(\frac{2\pi}{\lambda}\right)^2 \left(n^2 - n_{eff}^2\right) E = 0 \qquad \textbf{(1)}$$

$$\Delta_t^2 u_m + \left(\frac{\Omega_m^2}{V_l^2} - \beta_{acoust}^2\right) u_m = 0 \qquad \textbf{(2)}$$

where Δ_t is the transverse Laplacian operator in the (x,y) plane, $E(x,y)$ is the spatial distribution of the optical field, n_{eff} is the effective index of the fundamental LP_{01} optical mode, β_{acoust} is the acoustic propagation constant, $u_m(x,y)$ is the longitudinal displacement field of the L_{0m} acoustic mode and Ω_m is the acoustic Brillouin resonance frequency (i.e. Brillouin frequency shift). Assuming that Ω_m is much smaller than the optical frequency, the phase matching (i.e. Bragg condition) with the optical wave leads to the relation $\beta_{acoust} = 2\beta_{opt}$ where $\beta_{opt} = 2\pi n_{eff}/\lambda$ is the propagation constant of the optical mode [3].

The refractive index n and the longitudinal acoustic velocity V_l vary on the cross-section of the fiber according to the type and concentration of doping components. The fractional dependence for unit doping concentration on the optical and acoustical properties of pure silica is listed in Table 1 for most commonly used dopants. The acoustic velocity of pure silica is V_{silica}=5944m/s [10].

Table 1: Influence of doping concentrations on optical and acoustic properties of fibers parameters [10]

Doping	Δn%/wt.%	ΔV_l%/wt.%
GeO_2	+0.056	-0.47
F	-0.31	-3.6
P_2O_5	+0.020	-0.31
TiO_2	+0.23	-0.59
Al_2O_3	+0.063	+0.42
B_2O_3	-0.033	-1.23

The modal field distributions of both the LP_{01} optical mode and the L_{0m} acoustic modes determine the efficiency of the back-scattering wave. Fig. 1 plots the typical field distribution for two different L_{0m} acoustic modes. The acousto-optic coupling rate for the m^{th} acoustic mode can be expressed as [11]:

$$I_m^{ao} = \frac{\left(\int |E|^2 u_m * dxdy\right)^2}{\int |E|^4 dxdy . \int |u_m|^2 dxdy} \qquad \textbf{(3)}$$

Because of exponential decrease of acoustic waves, the spontaneous Brillouin spectrum of each acoustic mode has a Lorentzian shape. As each acoustic mode contribution adds up in an incoherent way, the BGS is then computed by adding lorentzian curves centered at each mode Brillouin frequency shift, $\nu_B^m = \Omega_m/2\pi$ with linewidth at half maximum Γ and relative intensity I_m^{ao}. Finally, the BGS $S(\nu)$ can be expressed as:

$$S(\nu) = \sum_m I_m^{ao} \frac{(\Gamma/2)^2}{(\Gamma/2)^2 + \left(\nu - \nu_B^m\right)^2} \qquad \textbf{(4)}$$

The Brillouin linewidth Γ is assumed to be 40MHz for every acoustic mode here.

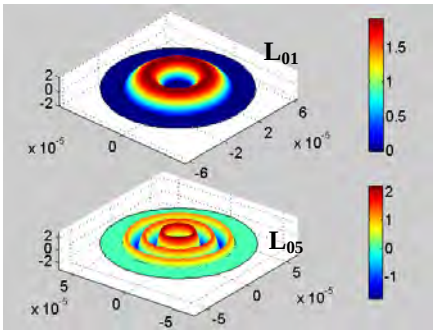

Figure 1: Examples of acoustic modes profiles for a Fluorine-doped cladding fiber

3. Simulation and use of COMSOL Multiphysics

3.1 2D-FEM Modeling

The optical parameters $E(x,y)$ and n_{eff}, and the mechanical parameters $u_m(x,y)$ and Ω_m are obtained separately by solving Eq. (1) and (2)

respectively using the PDE solver of COMSOL Multiphysics. The geometry, the (multi-)doping profile and eventually the stress distribution, are introduced in the PDEs. The number of elements of the mesh is varying between 10^4 and 10^6 depending of the complexity of the fiber geometry. The boundary condition is given by the perfectly matched layer for interior boundaries (i.e. Neumann boundary conditions: continuity of the fields and their derivative) and a restrictive trial space condition for the exterior boundaries (Dirichlet boundary condition: there is no field outside the fiber).

First, we calculate the optical mode profile $E(x,y)$ and the corresponding effective index n_{eff}. Note that the n_{eff} parameter is directly related to Brillouin frequency shift via the Bragg condition where V_{eff}^m is the effective acoustic velocity of the mth mode $\nu_B^m = 2n_{eff}V_{eff}^m/\lambda$. So, we can calculate the different longitudinal acoustic modes (in other words the different values of u_m and Ω_m) by introducing the value of n_{eff} in Eq. (2) according to the phase-matching condition. Finally, the acousto-optic overlap parameter I_m^{ao} is calculated using $E(x,y)$ and $u_m(x,y)$ (see Eq. 3), and the BGS $S(\nu)$ can be easily deduced.

3.2 Validation: GeO_2-doped core fibers

Our developed numerical model has been validated on the BGS determination of a commonly used fiber at 1.55µm, the SMF28 fiber. The fiber consists of a GeO_2-doped core fiber with a radius of 4.2µm and a doping concentration of 6% which corresponds to index variation of $\Delta(=\Delta n/n)=0.36\%$, and a pure silica cladding with radius 62.5µm. The index profile is given in Fig. 2. The phase velocity of the lower L_{om} acoustic modes have been calculated numerically and plotted in Fig. 3. The quasi-vertical line corresponds to the Bragg condition. It results that only four L_{om} acoustic modes are propagated in the fiber. All acoustic modes excepted L_{01} mode have non-zero cutoff frequencies. The field distributions of the LP_{01} optical and L_{om} acoustic modes are presented in Fig. 4.

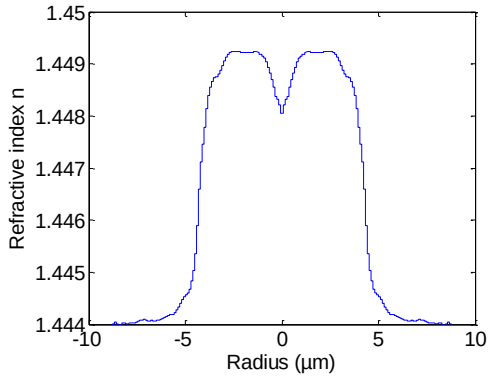

Figure 2: Measured refractive index profile of an SMF28 fiber

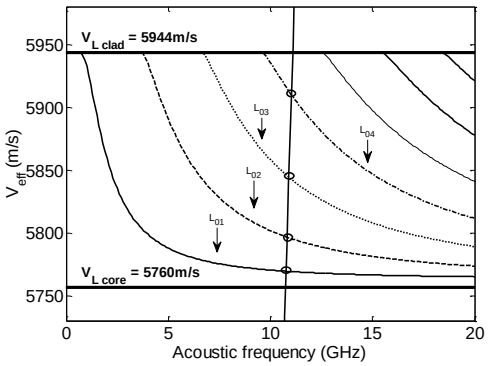

Figure 3: Calculated phase velocity of the lower acoustic modes L_{om} propagating along the GeO_2-doped core fiber (SMF28). The quasi-vertical line corresponds to the Bragg condition.

We have compared the calculated BGS with experimental results obtained on a ~10km SMF28 fiber. The BGS measurement has been performed using the well-known self-heterodyne technique [12, 13] (cf. experimental set-up in Fig. 5). A 1560nm DFB laser is used as the input signal. The heterodyne detection of both the Brillouin frequency shift back-propagated Stokes

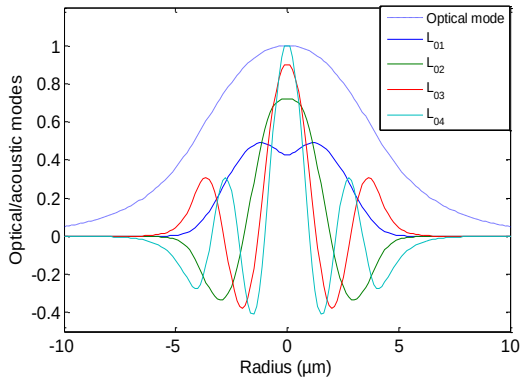

Figure 4: Profiles of the LP_{01} optical mode and the different L_{om} acoustic modes

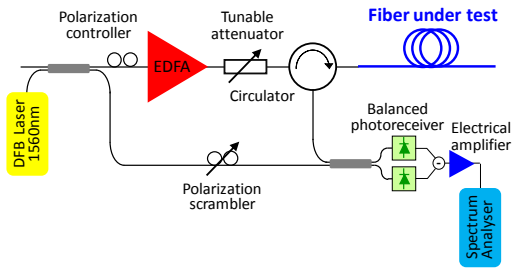

Figure 5: Experimental set-up for the measurement of Brillouin spectrum

wave in the fiber under test and the injected input signal allows to direct measurement of the BGS. A polarization scrambler is used in order to polarization insensitive measurement during the experiment. The laser linewidth is ~1 MHZ, compared to ~35-40MHz for the acoustic modes, so the detected electrical spectrum corresponds directly to the spontaneous BGS

The calculated BGS is in very good agreement compared with measurements as shown in Fig. 6. The BGS is composed of 4 peaks, each one corresponding to the contribution of a L_{0m} acoustic mode. The contribution of L_{01} acoustic mode is clearly dominant. The field distribution of the optical mode and fundamental L_{01} acoustic mode are similar as shown in Fig. 5, so the corresponding acousto-optic coupling rate I_1^{ao} is about 1. On the contrary, the field distributions of higher acoustic modes are composed of out-of-phase contribution, resulting in strongly reduced acousto-optic coupling rates. These experimental results confirm the accuracy of the 2D-FEM modeling.

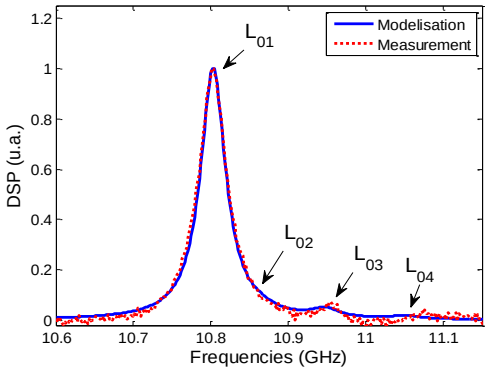

Figure 6: Comparison measurement/simulation of the BGS of an SMF28 fiber (~10km)

4. Fluorine-doped cladding fiber: case of acoustic anti-waveguides

The lowest fiber attenuation of 0.1484 dB/km has been achieved using pure silica core, Fluorine-doped cladding resulting in a depressed optical index [14]. Moreover, this fiber structure is interesting because Fluorine-doped cladding allows design of more sophisticated optical index profiles, for applications such as dispersion compensating fibers [15] or fibers with SBS (Stimulated Brillouin Scattering) mitigating [16] (i.e. the overlap between the optical and acoustic mode field is reduced). Until recently they are only few studies of the BGS analysis of pure-Fluorine doped cladding fibers [5, 9, 17].

The refractive index profile of the characterized Fluorine fiber is shown in Fig. 7. The fiber has a pure silica core of ~4.5µm radius and a Fluorine-doped cladding of ~43µm radius. The Fluorine doping in the cladding results in an acoustic velocity decrease. So, the acoustic waves are essentially confined in the cladding and not in the core. A Fluorine-doped cladding fiber acts as an acoustic anti-waveguide.

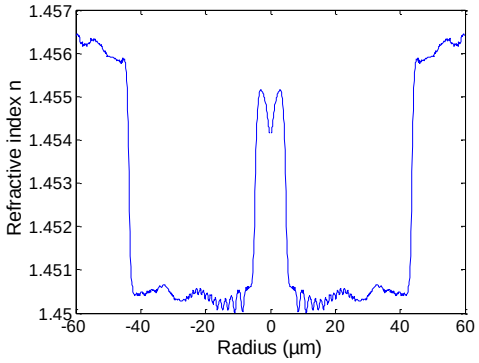

Figure 7: Measured refractive index profile of the Fluorine-doped cladding fiber

As we used the real profile with no approximation for 2D-FEM computation, it is necessary to have a highly thin mesh because of the composition of the fiber. COMSOL Multiphysics gives thousands of acoustic modes. As the optical mode distribution is no azimuthally dependent, only the acoustic modes with axially-symmetric field distribution should be taken into account. We select the acoustic modes with a significant overlap with optical

power distribution. Fig. 8 shows the radial profile of the acoustic mode with the highest value of I^{ao}.

The contributions of the most significant acoustic modes to BGS, as illustrated in Fig. 9,

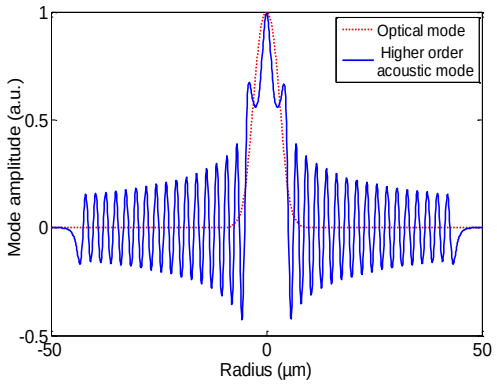

Figure 8: Radial profiles of the optical mode and the most efficient acoustic mode in the Fluorine doped fiber

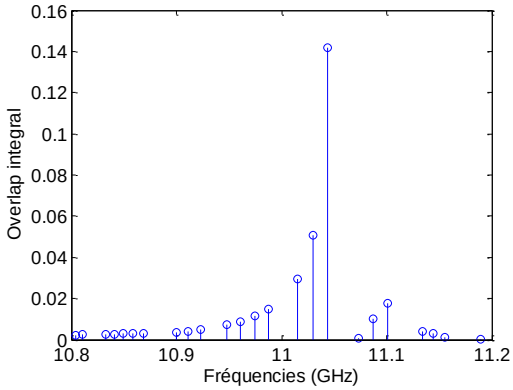

Figure 9: Values of the overlap integrals I_m^{ao} of acoustic modes with significant contribution to BGS

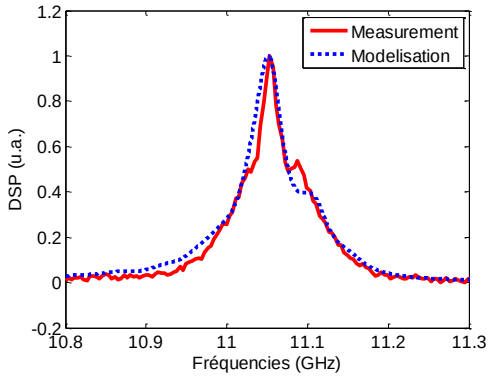

Figure 10: Measurement/simulation comparison of the BGS for a Fluorine-doped cladding fiber

show a predominant influence of modes around 11.05GHz. Both measured and calculated BGS are plotted in Fig. 10. The lower-order acoustic modes are confined in the inner region of the cladding. At the opposite, the upper-order acoustic modes are confined in the outer region of the cladding, so their coupling with the optical mode are non-significant compared to the lower-order modes around 11.05GHz.

5. Polarization-maintaining fibers

Polarization-maintaining fibers (PMFs) are used in many applications such as optical fiber communications when polarization control is required, fiber-optics sensors, interferometers, etc. PMFs have strong built-in birefringence. The most popular PMF design, also called PANDA fiber, consists in two stress rods on both sides of the fiber core as shown in Fig. 12. As PANDA fiber are no axially-symmetrical, 2D-FEM modeling is particularly adapted of the calculation of stress birefringence and BGS.

The cross-section geometry of the studied PANDA fiber is listed in [8]. Its structure consists in a GeO_2-doped core with radius a=4.225µm, a pure silica cladding with radius b=62.5µm and stress-applying elements around the core (see Fig. 11).

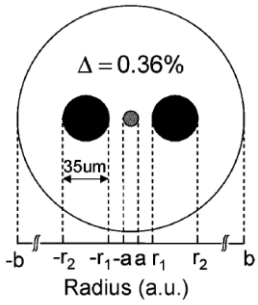

Figure 11: Cross-section of a PMF (PANDA fiber)

The finite element method and the modal resolution thanks to COMSOL Multiphysics allow us to calculate the thermal stress distribution (Fig. 12a and 12b). The stress components σ_x and σ_y in the fiber determine the spatial distribution of along x- and y-direction refractive indexes. The stress distributions could have been obtained using the *Structural Mechanics* Module of COMSOL. However for simplicity, we applied an analytical model that is

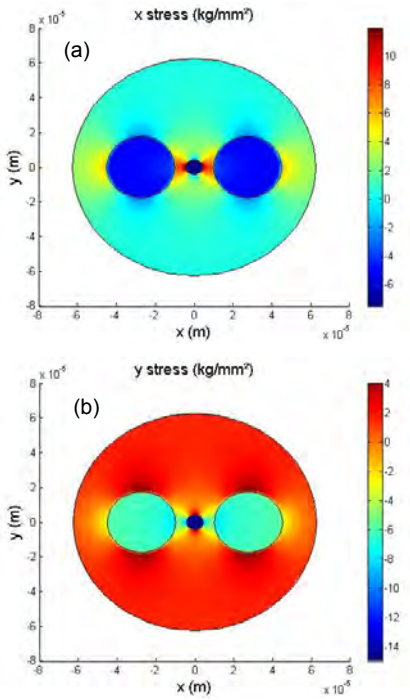

Figure 12: Stress distributions in the PANDA fiber cross-section: (a) x-axis, (b) y-axis.

described in [18]. Having found the stress components σ_x and σ_y, the corresponding stress induced birefringence can be easily deduced (i.e. birefringence B=C (σ_x - σ_y) where C is the stress-photoelastic coefficient of silica which is usually taken to be 3.36 10^{-5} mm^2/kg). The birefringence distribution for the considered PANDA fiber is shown in Fig. 13. Moreover, the stress modifies the longitudinal acoustic velocity as follows:

$$V'_l = V_l \sqrt{1 + \frac{1-2\gamma}{E}(\sigma_x + \sigma_y)} \qquad (5)$$

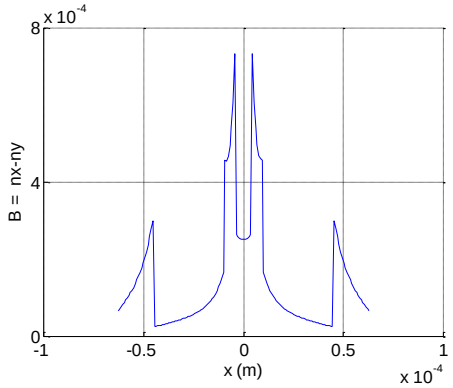

Figure 13: Birefringence profile along the x-axis

where V_l is the acoustic velocity in the core region for the no-stressed fiber [19]. The Young's modulus E=7830kg/mm² and the Poisson's ratio is $\gamma = 0.186$.

The calculated BGS with incident light along the slow axis (PMF-x) and fast axis (PMF-y) are plotted in Fig. 14. The BGS of the no-stressed fiber (i.e. no-stress applying elements) is shown for comparison. The BGS of the PMF on both x and y axis show a single-peak distribution, that can be explained by very close values of the Brillouin frequencies for the first four acoustic modes. The increase of the resonant frequencies from the no-stressed fiber to the PMF is approximately 53MHz, 7MHz corresponding to the stress induced dependence of n_{eff} (from 1.4603 to 1.4594), and 60MHz to the increase of V_l (from 5795.7m/s to 5827.8m/s). The difference of 2MHz between the PMF-x and PMF-y peaks is due to the birefringence induced by the Δn_{eff} between the two light propagation axis x and y.

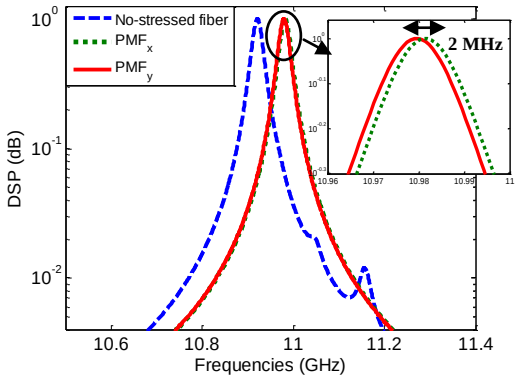

Figure 14: Stimulated BGS computed in the PANDA along x–polarization and y–polarization compared with the BGS in the no-stressed fiber

Note that our results are in good agreement with the spectrum measured experimentally in [8, 20]. In conclusion, we see that this approach is reliable even with non-symmetric fiber's structure.

6. Conclusions

We have demonstrated a 2D-FEM modal analysis to investigate the BGS in optical fibers. This model is particularly adapted for cladding

doped fibers that act as anti-waveguides and fibers with complicated 2D geometry and stress-induced refractive index profiles. We believe this method will be helpful designing and analyzing optical fibers for optical fiber communications and Brillouin-based fiber sensors.

7. References

1. V. Lanticq, R. Gabet, J.-L. Auguste, S. Délépine-Lesoille, S. Fortier and Y. Jaouën, "Spontaneous Brillouin scattering modeling and measurement in various axis-symmetric optical fibers", *ECOC 2007*, Berlin (2007)

2. G. Kulscar, Y. Jaouën, et al., "Multi-Stokes stimulated Brillouin scattering generated in pulsed high-power double cladding Er^{3+}/Yb^{3+} co-doped fiber amplifiers" *Photon. Technol. Lett.,* vol. 15, pp. 801-803 (2003)

3. G.P. Agrawal, "Nonlinear Fiber Optics". Academic Press (2006)

4. D.A Fishman and J.A. Nagel, "Degradations due to stimulated Brillouin scattering in multigigabit intensity-modulated fiber-optic systems", *Lightwave Technol.,* vol. 11, pp. 1721-1728 (1990)

5. W. Zou, Z. He, M. Kishi, and K. Hotate, "Stimulated Brillouin scattering and its dependences on temperature and strain in a high-delta optical fiber with F-doped depressed inner-cladding," *Opt. Lett.*, **32**, pp. 600–602, March 2007.

6 K.Y. Song, M.G. Herraez and L. Thevenaz, "Observation of pulse delaying and advancement in optical fibers using stimulated Brillouin scattering," *Opt. Express,* **13**, pp.82-88 (2005)

7. Y. Koyamada, S. Sato, S. Nakamura, H. Sotobayashi, and W. Chujo, "Simulating and designing Brillouin gain spectrum in single-mode fibers," *Lightwave Technol.*, vol. 22, pp. 631–639 (2004)

8. W. Zou, Z. He and K. Hotate, "Two-dimensional finite-element modal analysis of Brillouin gain spectra in optical fibers" *Photon. Technol. Lett*., vol.18, pp. 2487-2789 (2006).

9. L. Tartara, C. Codemard, J.-N. Maran, R. Cherif and M. Zqhal, "Full modal analysis of the Brillouin gain spectrum of an optical fiber*"* *Optics Com*., vol. 282, pp. 2431-2436 (2009)

10. C. K. Jen, A. Safaai-Jazi and G.W Farnell, "Leaky modes in weakly guiding fiber acoustic waveguide" *IEEE Trans*. Ultrason., Ferroelectr. Freq., Control., vol. 33, pp. 634-643 (1986)

11. A. Kobyakov, S. Kumar et al., "Design concept for optical fibers with enhanced SBS threshold" *Opt. Express***, 13**, pp. 5338-5346 (2005)

12. A. Yeniay, J. M. Delavaux, and J. Toulouse. "Spontaneous and stimulated Brillouin scattering gain spectra in optical fibers" *Lightwave. Technol.*, vol. 20, pp. 1425-1432 (2002)

13. V. Lanticq, S. Jiang, R. Gabet, T. Jaouën, et al. "Self-referenced and single-ended method to measure Brillouin gain in monomode optical fibers" *Opt. Lett.*, **34**, pp. 1018-1020 (2009)

14. K. Nagayama, M. KaKui, M. Matsui, T. Saiyoh and Y. Chigusa, "Ultra-low-loss (0.1484 dB/km) pure silica core fiber and extension of transmission distance" *Electron. Lett.*, Vol. 38, pp. 1168-1169 (2002)

15. T. Sasaki, K. Makihara, M. Hirano, et al., "Novel dispersion compensation fiber with fluorine-doped cladding for simultaneous realization of high dispersion compensation efficiency and low attenuation" *OFC'2006*, paper OThA2 (2006)

16. M.-J. Li, X. Chen, J. Wang, et al, "Fiber designs for reducing stimulated Brillouin scattering" *CLEO'2006*, paper OTuA4 (2006)

17. Y. Koyamada, S. Sato, et al. , "Simulating and designing Brillouin gain spectrum in single-mode fibers" *Lightwave Technol.*, vol. 22, pp. 631-639 (2004)

18. P. L. Chu and R. A. Sammut, "Analytical method for calculation of stresses and material birefringence in polarization-maintaining optical fiber" *Lightwave Technol.*, vol. 2, pp. 650–662 (1984)

19. S. P. Timoshenko and J. N. Goodier*, Theory of Elasticity*, 3rd ed. New York: McGraw-Hill (1970)

20. Q. Yu, X. Bao and L. Chen, "Temperature dependence of Brillouin frequency, power, and bandwidth in panda, bow-tie, and tiger polarization-maintaining fibers" *Opt. Lett.*, **29**, pp. 17-19 (2004)